Int. J. Electrochem. Sci., 7 **(2012)** 8369 - 8383

International Journal of
ELECTROCHEMICAL
SCIENCE
www.electrochemsci.org

Isothermal Oxidation Behavior Characteristics of a Second Generation Ni-base Single Crystal Superalloy in Air at 1000 and 1100°C

Fahamsyah H. Latief[*], *Koji Kakehi, Xintao Fu, Yuma Tashiro*

Department of Mechanical Engineering, Tokyo Metropolitan University, 1-1 Minami-osawa, Hachioji-shi, Tokyo 192-0397, Japan
[*]E-mail: fahamsyah78@gmail.com

Received: 18 July 2012 / *Accepted:* 15 August 2012 / *Published:* 1 September 2012

The isothermal oxidation behavior of a second generation Ni-base single crystal superalloy was investigated in air at 1000°C and 1100°C. The microstructures of the oxide morphology and the cross-section area of the specimens after oxidation were analyzed by XRD and SEM/EDX. Indeed, the present results indicated that the Ni-base single crystal superalloy denoted the parabolic oxidation kinetics, which are primarily controlled by the growth of the inner α-Al_2O_3 layer. In conclusion, the scales formed on the surface of superalloy both at 1000°C and 1100°C were complex and can be classified into three different layers in general: an outer layer of NiO with a small amount of CoO, an intermediate layer which predominantly composed of spinels $(Ni,Co)Al_2O_4$, $NiCr_2O_4$, and accompanied with some other oxides such as $CrTaO_4$, $NiTiO_3$ as well as $W_{20}O_{58}$, and an inner continuous layer of α-Al_2O_3. Nevertheless, the poor Al zone was appeared between the oxide scales and the substrate after oxidation 200 h and 500 h both at 1000°C and 1100°C.

Keywords: single crystal Ni-based superalloy, oxidation behavior, microstructure, surface morphology

1. INTRODUCTION

Ni-based single crystal superalloys have been widely used as turbine blade materials for advanced aircraft engines. The materials with their superior performance both in mechanical strength and oxidation resistance are required to be applied for high temperature applications [1-3]. Recently, the surface operating temperatures of gas-turbine blades could reach up to 1100°C or even higher. However, high operating temperature motivates the degradation of superalloys during service with respect to oxidation or corrosion behavior [4,5]. At high temperature, the oxidation resistance behavior of the materials becomes one of the major life-limiting factors.

Poor oxidation resistance will constitute severe degradation to the service life of superalloy and propose great threat to the service reliability of an engine [6,7]. Nowadays, several alloying elements was added through the solid solution hardening method and Al and Ta via formation of a γ′ precipitate in a γ nickel matrix in order to improve the mechanical properties of superalloys, [8,9]. The alloy contains refractory elements such as W, Ta, Cr and Co to prevent local hot corrosion, and Re addition can improve the oxidation [10]. In some cases, carbon is also used to improve the grain boundary properties [11] while Al and Cr are added to optimize the oxidation resistance. It is necessary to identify the intrinsic behavior of the substrate in oxidizing atmosphere. Therefore, investigation on oxidation behavior of single crystal superalloys becomes important. In the present study, the isothermal oxidation behavior of Ni-based single crystal superalloy at 1000°C and 1100°C in air was investigated.

2. EXPERIMENTAL DETAILS

A second generation of Ni-base single crystal superalloy was used as a substrate material in this study. The nominal chemical composition of superalloy is 5.74 Al, 0.73 Ti, 6 Cr, 9.3 Co, 1.4 Hf, 3.4 Ta, 2.9 Re, 8.3 W, 0.005 Zr, 0.016 B, 0.019 Fe, 0.07 C and balance Ni in mass%. For this intention, a cylindrical rod of superalloy was directionally solidified in [001]-direction. The heat treatment of cylindrical rod was carried out according to following heat treatment regime: at 1080 °C for 4 h and at 871 °C for 20 h, both treatments followed by gas fan cooling. The specimen was then cut from the rod along the (001) orientation with the dimension of 10 mm in length, 5 mm in width and 3.5 mm in thickness by electro discharge machine (EDM).

Prior to isothermal oxidation testing, the specimens were mechanically polished down to 1200-grit SiC paper, degreased in acetone, ultrasonically cleaned in alcohol and dried in air. Isothermal oxidation kinetic tests were conducted at 1000°C and 1100°C for 500 h in air environment. The oxidation kinetics was experimentally measured as a function of weight gain against oxidation time. During oxidation, the mass gain of the specimens was quantified discontinuously. The sensitivity of the electron balance (Shimadzu) used in this study was 0.1 mg.

The phase constitutions of oxidation layers after oxidation on the surface of superalloy were determined by X-ray diffraction (Rigaku) using Cu Kα radiation. The initial microstructure of superalloy was observed by optical microscope (Olympus). Then, the surface morphology and cross-section of superalloy after oxidation were analyzed by a HITACHI scanning electron microscope equipped with energy-dispersive X-ray analysis (EDX).

3. RESULTS AND DISCUSSION

3.1. Oxidation kinetics

The isothermal oxidation kinetics of superalloy performed at 1000°C and 1100°C is shown in Fig. 1. The results exhibited that the superalloy has better oxidation behavior at 1000°C than that at

1100°C. It was apparent from the mass gain of the specimens obtained at both temperatures in the initial oxidation period of 25 h where the mass gain was rapidly increased due to the free surface of superalloy. This stage is named as formation period of the oxide film. With increasing oxidation time, the mass gain of the specimens was gradually increased and the growth of oxidation film started during this period.

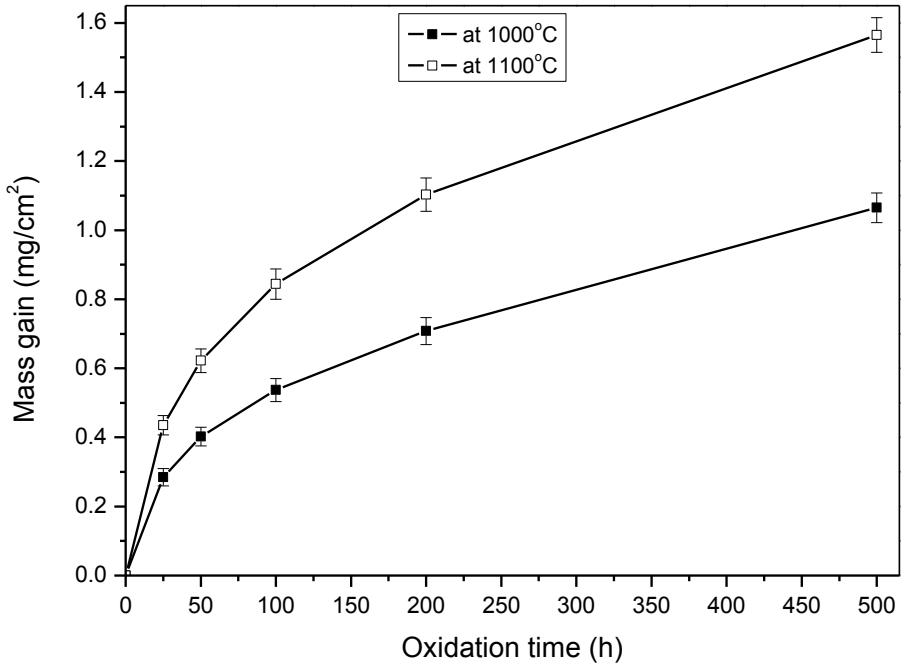

Figure 1. Oxidation kinetics curve of Ni-base single crystal superalloy after oxidation at 1000°C and 1100°C.

The previous work [12] reported where the increase of the mass gain and the thickness of oxide layer follow a square power law for diffusion-controlled oxidation behavior. Thus, the parabolic rate constant K_p of superalloy can be assessed by a linear least-squares algorithm from the following equation [13]:

$$(\Delta m/A)^2 = K_p . t \quad (1)$$

where Δm is the mass change (mg), A is the specimen surface area (cm^2), t is oxidation time (s) and K_p is the parabolic rate constant which can be directly estimated by plotting the square of the mass gain (mg^2/cm^4) over exposure time. The square of mass gain obtained had a nearly linear line as shown in Fig. 2. The results indicated that the oxidation kinetics at both 1000°C and 1100°C followed a parabolic oxidation law. Furthermore, the parabolic oxidation rate constants (K_p) and thus the oxidation rates of the superalloy in air are determined from the slope of $(\Delta m/A)^2$ vs t are 6.3 x 10^{-7} $mg^2cm^{-4}s^{-1}$ at 1000°C and 3.5 x 10^{-6} $mg^2cm^{-4}s^{-1}$ at 1100°C.

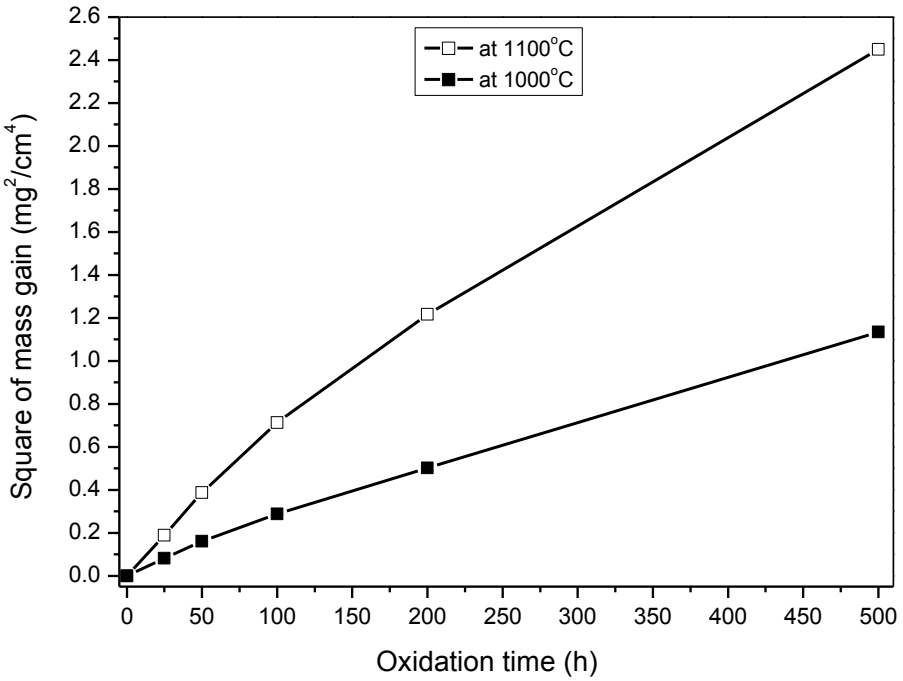

Figure 2. Square of the mass gain per unit area vs oxidation time for Ni-base single crystal superalloy after oxidation at 1000°C and 1100°C.

As previously reported, the oxidation kinetics of Ni-base single crystal superalloys obeys the parabolic law between the temperatures of 800°C and 1100°C [14]. As seen in Fig. 1, the oxidation kinetics of Ni-base single crystal superalloy in this paper nearly follows the parabolic law [14,15]. It is clear that the oxidation temperatures affected the oxidation rates of the superalloy as shown in Fig. 2 where the parabolic oxidation rate constants (K_p) value at 1100°C is higher than that at 1000°C.

3.2. Initial Microstructure

Fig. 3 shows the optical and SEM micrographs of superalloy. A Ni-base single crystal superalloy composed of 70–80% volume fraction of the γ′ phase. There are two different areas can be distinguished in which termed as dendritic and interdendritic as shown in Fig. 3a. Dendritic areas consisted of γ′ precipitates that are uniformly distributed in the γ matrix whereas the interdendritic areas generally contained γ′ and there was a dark region between dendritic and interdendritic (as indicated by the white arrow in Fig. 3a) which is consisted of γ′+γ eutectic precipitates in the γ matrix [11]. The enlarged eutectic region (as indincated by white arrow in Fig. 3a) is shown in Fig. 3b. In addition, the cuboidal γ′ precipitates aligned along <001> during the aging treatment due to the elastic interaction between precipitates and its configurations as shown in Fig. 3c. The size of cuboidal γ′ precipitates was varied between 0.5 to 1.75 μm.

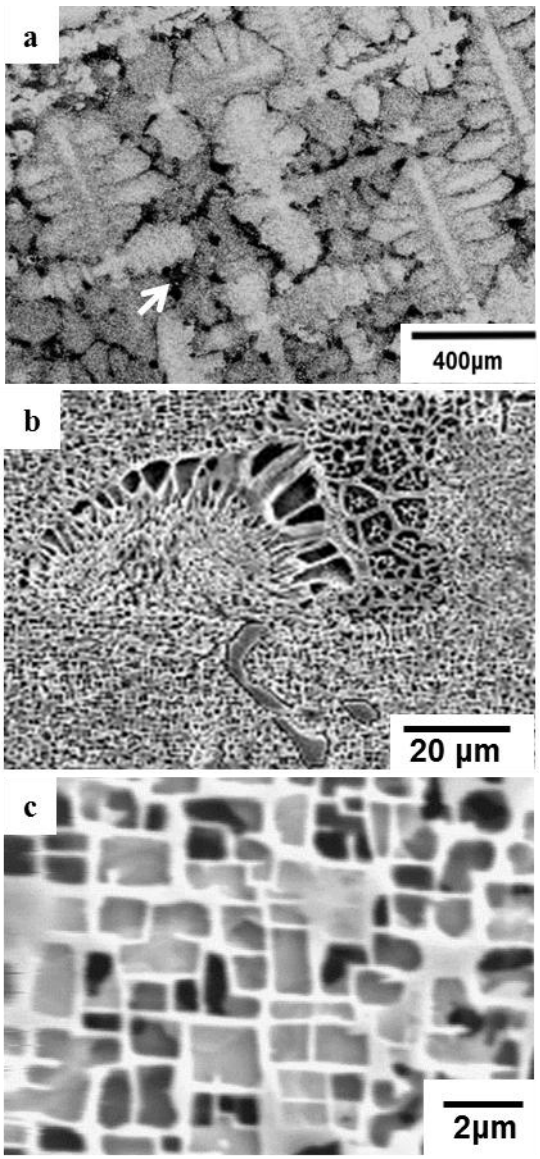

Figure 3. Optical and SEM micrographs of Ni-base single crystal superalloy: (a) dendrite structure, (b) eutectic region and (c) γ′ cuboidal precipitates in γ matrix.

3.3. X-ray diffraction

Fig. 4 and 5 present the XRD results of the surface of Ni-base single crystal superalloy after oxidation at 1000°C and 1100°C, respectively. After 200 h oxidation at 1000°C, the oxide products formed on the surface of superalloy were mainly α-Al_2O_3 accompanied with (Ni,Co)O and some spinels $NiCr_2O_4$, (Ni,Co)Al_2O_4, $NiTiO_3$ and $CrTaO_4$ with a small amount of a complex oxide $W_{20}O_{58}$ and HfO_2 precipitates. Whereas after 500 h oxidation at 1000°C, the oxidation products were quite similar to that for 200 h, but the amount of some oxides such as α-Al_2O_3, (Ni,Co)Al_2O_4, etc increased as indicated by the enhancement of peak intensity in XRD pattern as shown in Fig. 4. Meanwhile, after oxidation at 1100°C, in comparison with the oxidation products at 1000°C, the amount of α-Al_2O_3 and spinels such as (Ni,Co)Al_2O_4, $NiCr_2O_4$ and $CrTaO_4$ escalated with increasing the temperature and

oxidation time. Otherwise, the amount of (Ni,Co)O decreased with increasing the temperature due to the continuous reaction with α-Al_2O_3 to produce the spinel (Ni,Co)Al_2O_4 as shown in Fig. 5.

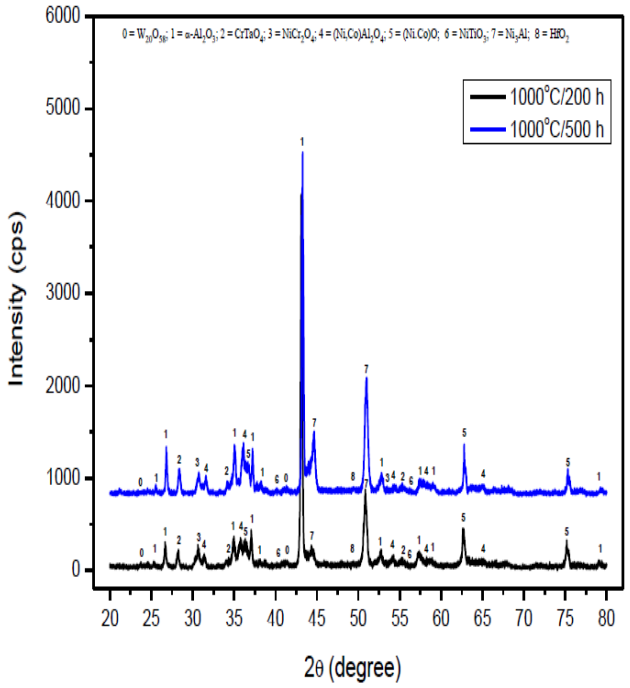

Figure 4. XRD patterns of Ni-base single crystal superalloy after 200 h and 500 h oxidation at 1000°C.

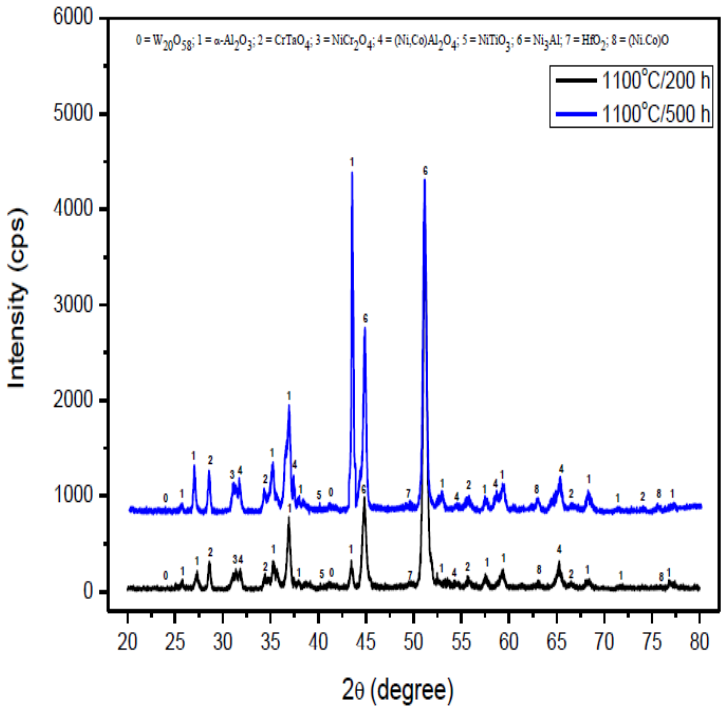

Figure 5. XRD patterns of Ni-base single crystal superalloy after 200 h and 500 h oxidation at 1100°C.

3.4. Surface morphology of oxides

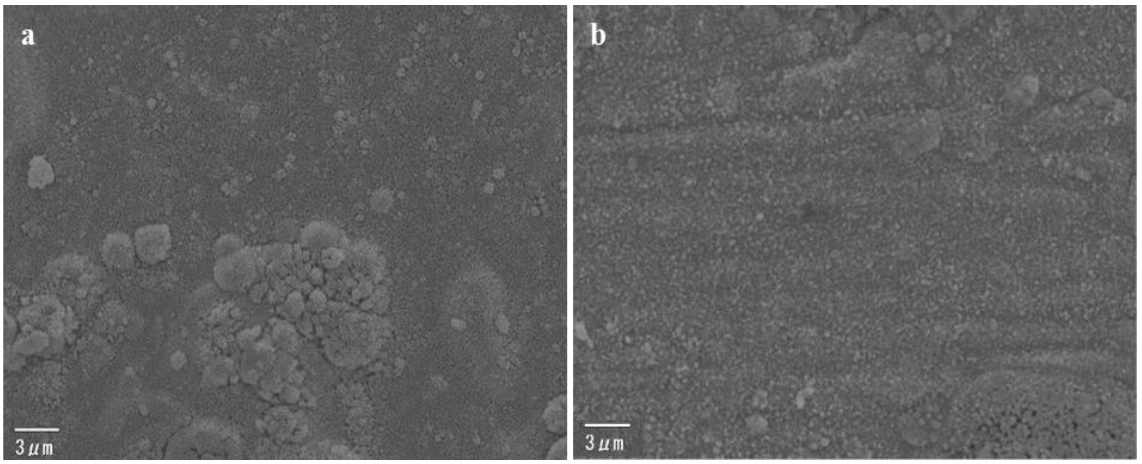

Figure 6. Surface morphologies of Ni-base single crystal superalloy after 25 h oxidation: (a) at 1000°C and (b) at 1100°C.

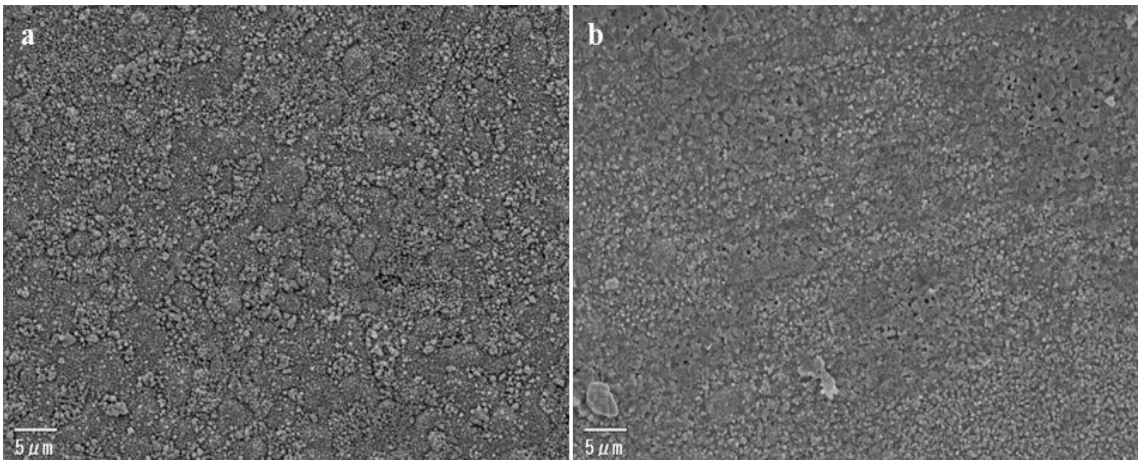

Figure 7. Surface morphologies of Ni-base single crystal superalloy after 50 h oxidation: (a) at 1000°C and (b) at 1100°C.

Surface morphology of oxide products formed on the surface of superalloy after oxidation at 1000°C and 1100°C is shown in Fig. 6 – 9. After oxidation for 25 h, the oxide products formed has very fine particle size with a high oxidation rate at both temperatures. The oxides were fully covered the surface of the specimens as seen in Fig. 6. After 50 h oxidation, the oxide particles were being coarsened at both temperatures as seen in Fig. 7. It can be readily recognized from the increase of oxide particles grain size with increasing the oxidation time where the grain size of oxide particles was about 200 nm to 400 nm at 1000°C and 350 nm to 1 μm at 1100°C. After oxidation for 200 h, the NiO particles were apparent and randomly distributed on the surface of superalloy at both temperatures as seen in Fig. 8. However, the NiO particles grew become larger than previous condition and spread over the surface of superalloy after 500 h at 1000°C and 1100°C as shown in Fig. 9. Nevertheless, it can be

obviously seen that NiO has a porous structure and blocky morphology. The grain size of NiO after 500h oxidation was varied between 0.4 μm to 4.5 μm at 1000°C and 0.5 μm to 6.5 μm at 1100°C.

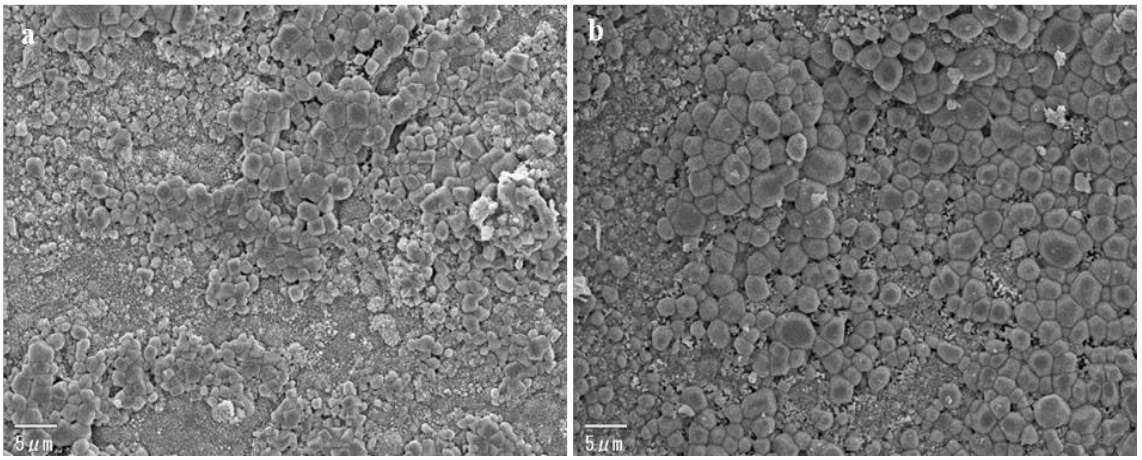

Figure 8. Surface morphologies of Ni-base single crystal superalloy after 200 h oxidation: (a) at 1000°C and (b) at 1100°C.

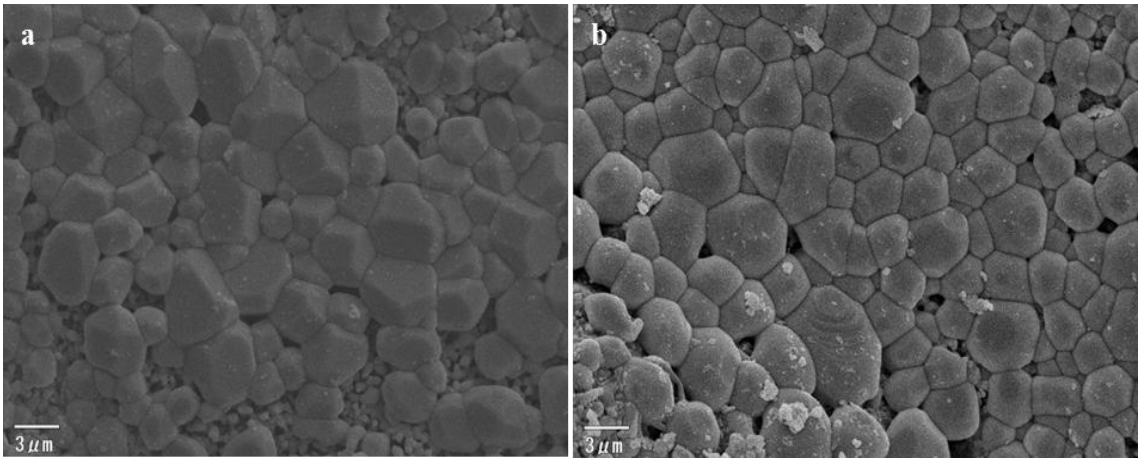

Figure 9. Surface morphologies of Ni-base single crystal superalloy after 500 h oxidation: (a) at 1000°C and (b) at 1100°C.

3.5. Cross-section microstructures after oxidation

The SEM micrographs of cross-section back-scattered electron image (BEI) with the corresponding energy dispersive X-ray (EDX) of the scale formed on the CM186LC superalloy after 200 h and 500 h oxidation at 1000°C and 1100°C are presented in Fig. 10 – 13, respectively. The BEI image was used in this investigation in order to augment the atomic number contrast in the oxidation products. The oxide scale formed at 1000°C and 1100°C was complex with its configurations and both can be divided into several layers. In addition, the detailed EDX results of the specimens after 200 h and 500 h oxidation at 1000°C and 1100°C was summarized in Table 1 and 2, respectively.

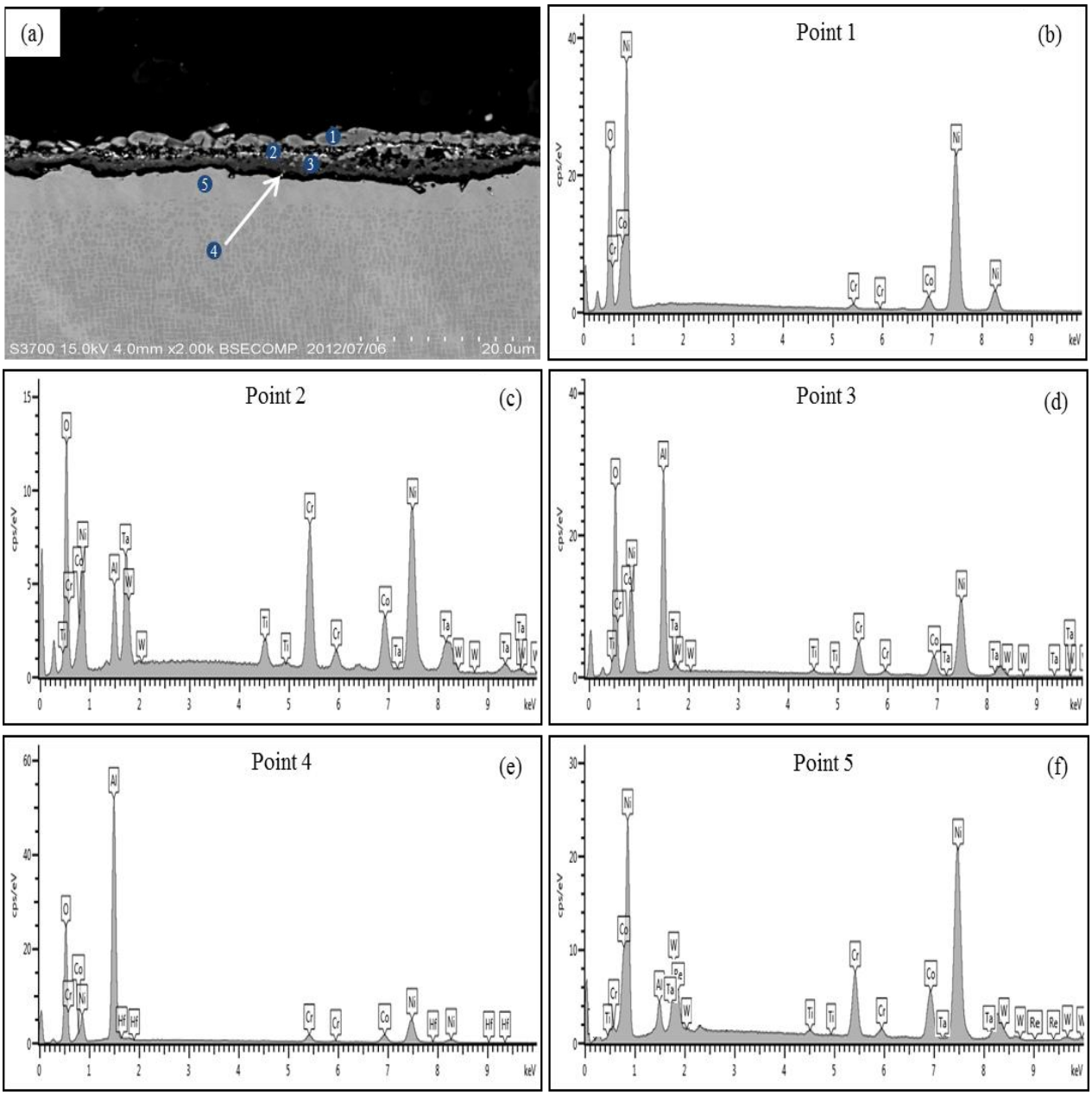

Figure 10. Cross-sectional SEM image of Ni-base single crystal superalloy: (a) after 200 h oxidation at 1000°C, whereas (b-f) represent the corresponding EDX profile analysis derived from points 1-5 for micrograph shown in (a).

Generally, the oxide scale formed on the surface at 1000°C and 1100°C consisted of an outer layer was made of NiO layer with a small amount of CoO (point 1), an intermediate layer which can be classified into two layers (points 2 and 3), an inner layer was composed of α-Al_2O_3 continuous layer which appeared as dark areas at the bottom of oxide scale combined with a small amount of HfO_2 precipitate (point 4) as shown in Fig. 10 – 13. After 200 h oxidation at 1000°C, the thickness of oxide scale formed was about 4 to 7.5 μm. The first intermediate layer mainly composed of (Ni,Co)Al_2O_4, $CrTaO_4$, $NiCr_2O_4$ with some small amounts of $NiTiO_3$ and $W_{20}O_{58}$, whereas the second intermediate layer predominantly consisted of (Ni,Co)Al_2O_4, $NiCr_2O_4$ with a small amount of $CrTaO_4$ as shown in Fig. 10. After 500 h oxidation at 1000°C, the thickness of oxide scale increased by extending the

oxidation time to be about 5.2 μm to 10.8 μm. Moreover, the first intermediate layer mainly composed of $(Ni,Co)Al_2O_4$, $CrTaO_4$, $NiCr_2O_4$ with some small amounts of $NiTiO_3$ and $W_{20}O_{58}$, whereas the second intermediate layer predominantly consisted of $(Ni,Co)Al_2O_4$ with a small amount of $NiCr_2O_4$ as shown in Fig. 11.

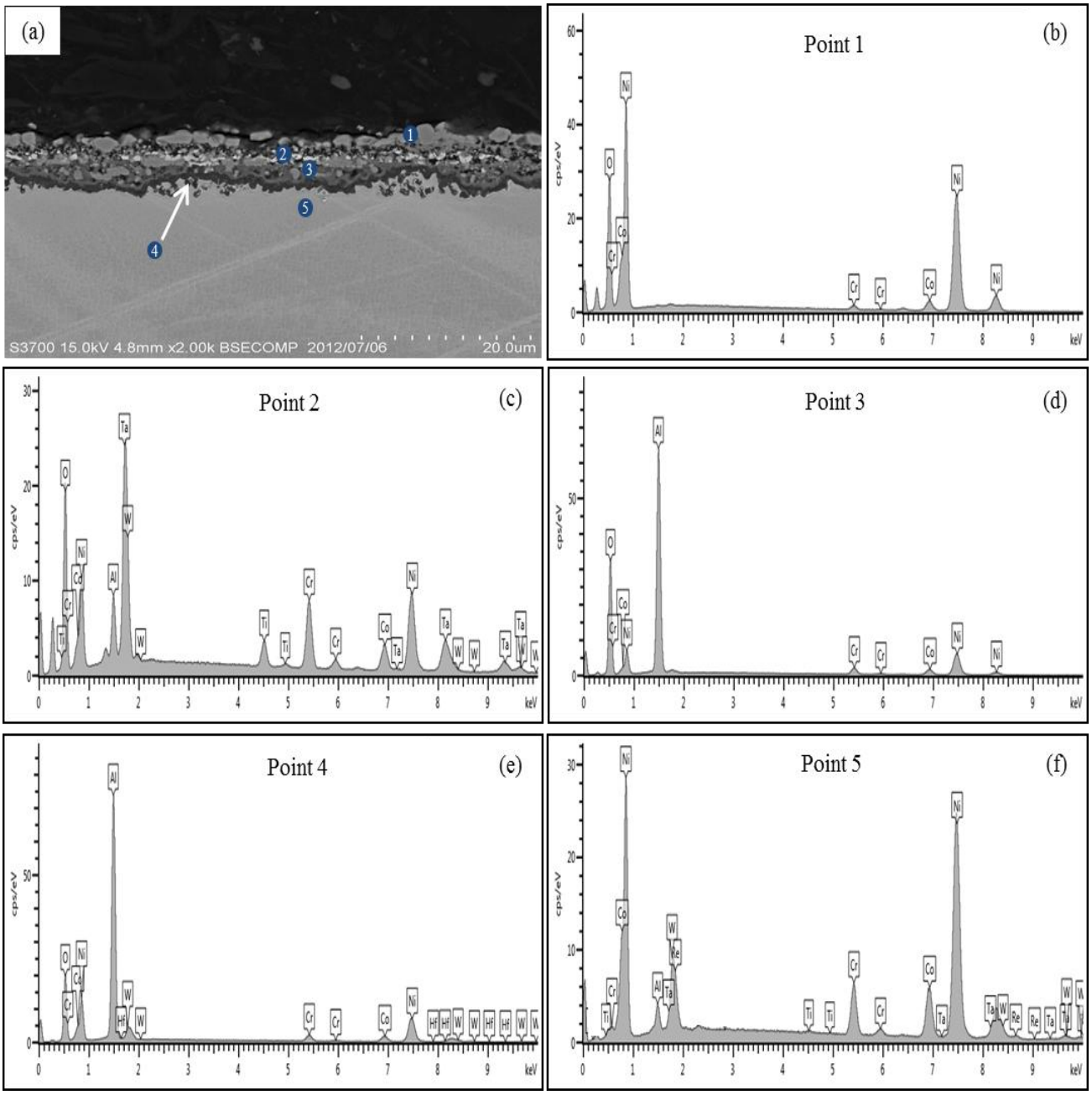

Figure 11. Cross-sectional SEM image of Ni-base single crystal superalloy: (a) after 500 h oxidation at 1000°C, whereas (b-f) represent the corresponding EDX profile analysis derived from points 1-5 for micrograph shown in (a).

At 1100°C for a duration of 200 h oxidation, the thickness of the entire oxide scale ranged from 5.6 μm to 8.4 μm. The first intermediate layer mainly composed of $(Ni,Co)Al_2O_4$, $CrTaO_4$, $NiCr_2O_4$

with a small amount of $NiTiO_3$ and $W_{20}O_{58}$, whereas the second intermediate layer predominantly consisted of $(Ni,Co)Al_2O_4$, $NiCr_2O_4$ with some small amounts of $CrTaO_4$ and $W_{20}O_{58}$ as shown in Fig. 12. Additionally, the complex oxide scale formed at 1100°C after 500 h oxidation was between 9.7 µm and 14.7 µm. The first intermediate layer at 1100°C after 500 h oxidation was similar to the condition at 1100°C for a duration of 200 h oxidation, but the amount of spinels $(Ni,Co)Al_2O_4$, $NiCr_2O_4$ and $NiTiO_3$, a complex oxide $CrTaO_4$ and $W_{20}O_{58}$ after 500 h was somewhat higher than after 200 h oxidation. Whereas the second intermediate layer predominantly consisted of $(Ni,Co)Al_2O_4$, $NiCr_2O_4$ with a small amount of $CrTaO_4$ and $NiTiO_3$ as shown in Fig. 13. In addition, the poor Al zone was found between the oxide scales and the substrate at 1000°C and 1100°C after 200 h and 500 h oxidation as shown in Fig. 10 – 13 (point 5).

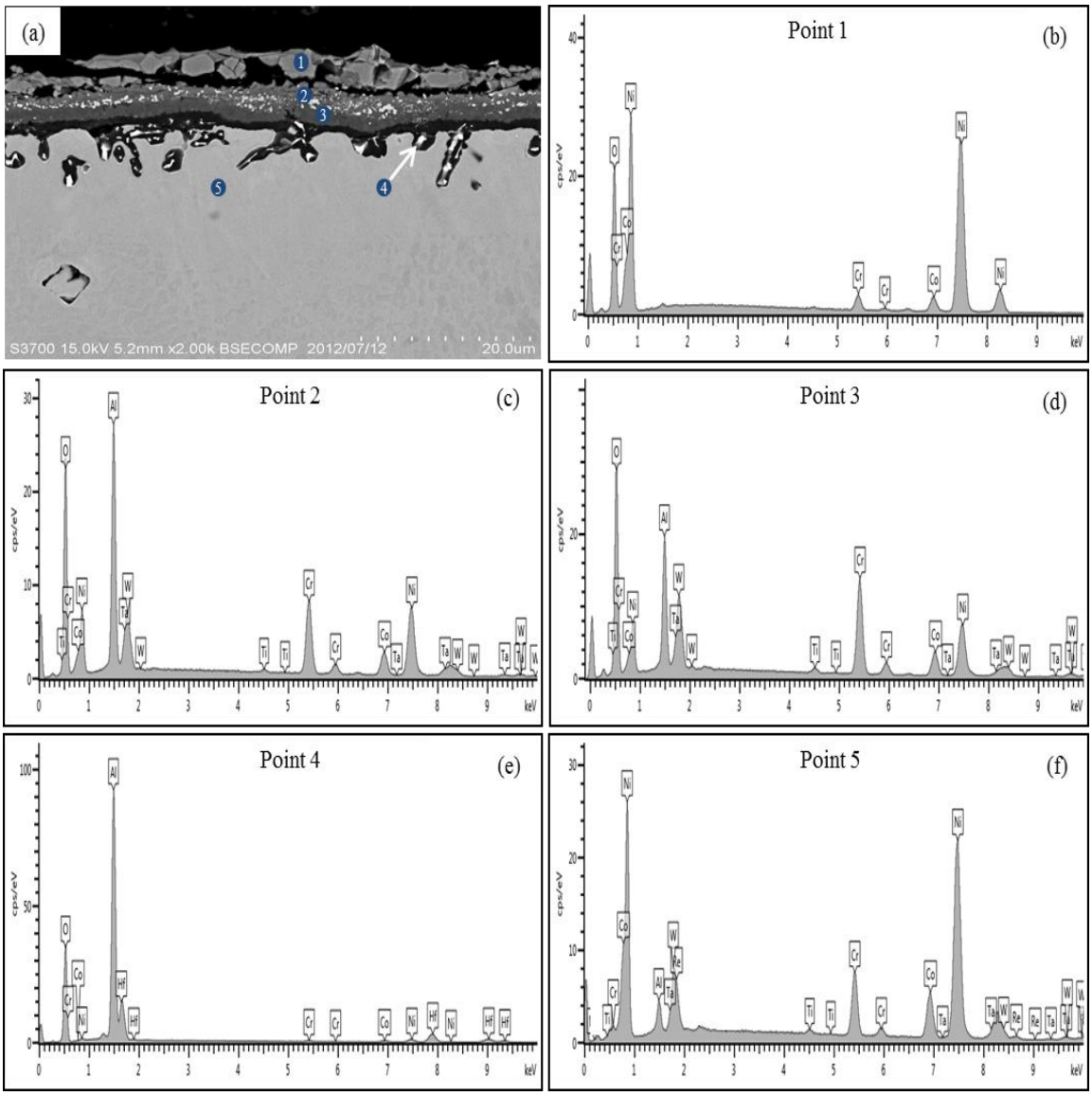

Figure 12. Cross-sectional SEM image of Ni-base single crystal superalloy: (a) after 200 h oxidation at 1100°C, whereas (b-f) represent the corresponding EDX profile analysis derived from points 1-5 for micrograph shown in (a).

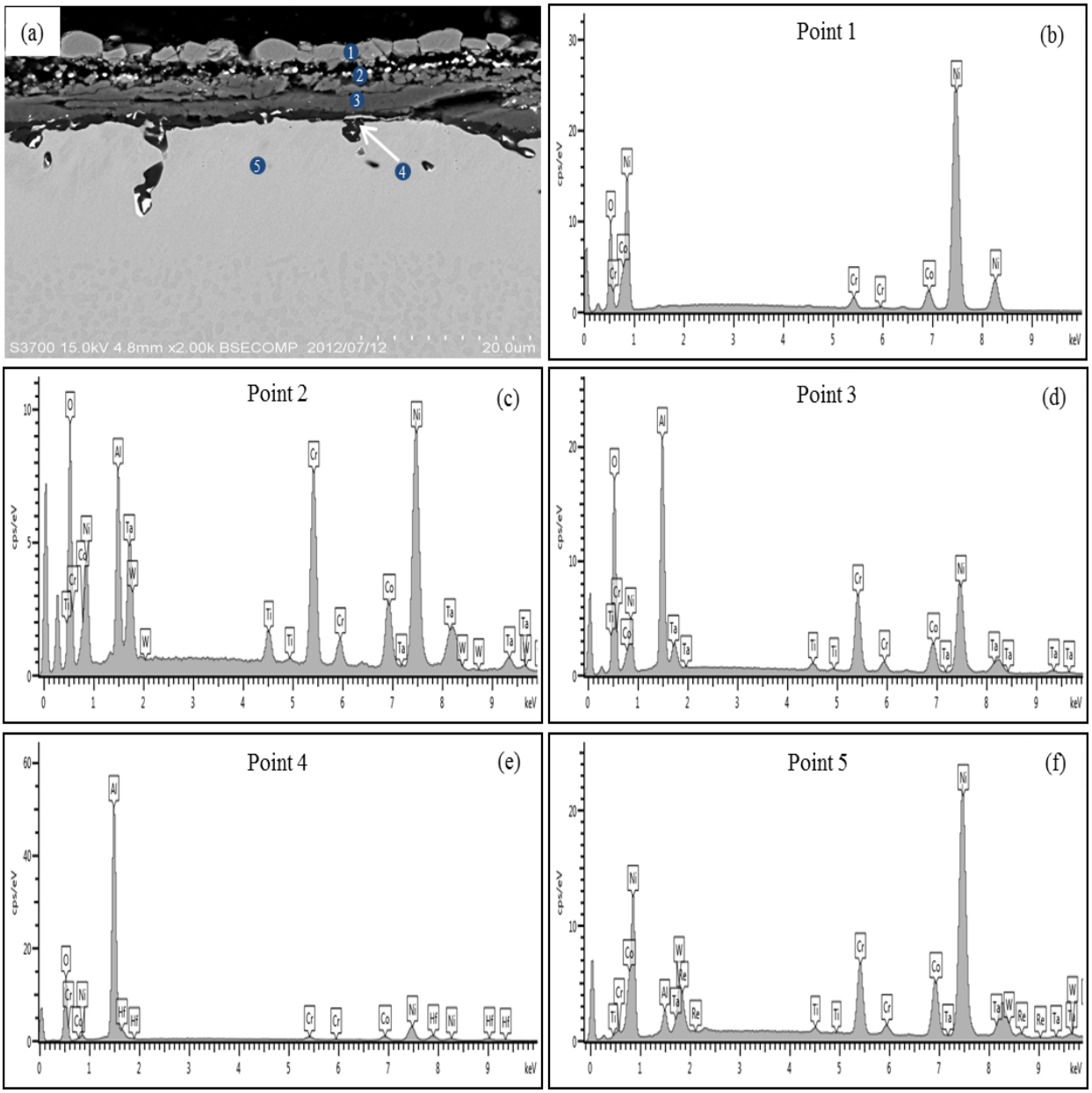

Figure 13. Cross-sectional SEM image of Ni-base single crystal superalloy: (a) after 500 h oxidation at 1100°C, whereas (b-f) represent the corresponding EDX profile analysis derived from points 1-5 for micrograph shown in (a).

3.6. Formation of oxide scales

Throughout the initial stage of oxidation at 1000°C and 1100°C, NiO formed at the outer dendritic area, the results obtained in this study are the same as reported by Giggins and Pettit [16]. The oxide was grown to form a film consisting of NiO with a small amount of CoO, which thickened by the solid-state diffusion due to a continuous reaction occurred during exposure. The simple oxides such as NiO, CoO, Al_2O_3 and others are also formed during the initial oxidation stage but the transient-oxidation period was quite short because of the rapid build-up of the inner α-Al_2O_3. This is due to Al has a very high oxygen affinity compared to other elements as described in Richardson–Ellington

diagrams [17,18]. In consequence, the Al is preferably oxidized. The oxygen penetrated into the NiO layer and diffused towards the superalloy and then reacted with Al and other atoms at oxide/superalloy interface diffusing from the superalloy to form Al_2O_3 and other particles in a region under scale/superalloy interface. Therewith, the rate of reaction then became determined by the transport through this growth layer.

Table 1. Chemical content of main elements in typical phase zone after oxidation at 1000°C (at.%) in Fig. 10 and 11

Condition	Points of no.	Element content (at.%)										Note
		O	Ni	Al	Cr	Co	Ti	W	Ta	Hf	Re	
1000°C/200 h (Fig. 10)	1	41.26	54.14	-	0.54	4.06	-	-	-	-	-	NiO+CoO
	2	35.34	29.20	4.90	14.25	8.82	2.23	2.37	2.89	-	-	$(Ni,Co)Al_2O_4+CrTaO_4+NiCr_2O_4+NiTiO_3+W_{20}O_{58}$
	3	45.49	23.96	19.76	4.94	5.07	0.12	0.07	0.57	-	-	$(Ni,Co)Al_2O_4+NiCr_2O_4+CrTaO_4$
	4	53.29	1.73	38.76	0.4	0.44	-	-	-	5.38	-	α-$Al_2O_3+HfO_2$
	5	-	66.64	3.72	11.39	13.14	0.57	2.52	0.47	-	1.2	Poor Al-zone
1000°C/500 h (Fig. 11)	1	43.95	51.56	-	0.58	3.91	-	-	-	-	-	NiO+CoO
	2	46.02	21.06	5.06	10.3	5.79	3.13	1.85	6.79	-	-	$(Ni,Co)Al_2O_4+NiCr_2O_4+CrTaO_4+NiTiO_3+W_{20}O_{58}$
	3	48.94	11.53	35.24	1.84	2.45	-	-	-	-	-	$(Ni,Co)Al_2O_4+NiCr_2O_4$
	4	34.76	11.05	46.14	1.02	1.96	-	0.02	-	5.05	-	α-$Al_2O_3+HfO_2$
	5	-	70.23	3.05	8.4	13.5	0.23	2.94	0.19	-	1.14	Poor Al-zone

Table 2. Chemical content of main elements in typical phase zone after oxidation at 1100°C (at.%) in Fig. 12 and 13

Condition	Points of no.	Element content (at.%)										Note
		O	Ni	Al	Cr	Co	Ti	W	Ta	Hf	Re	
1100°C/200 h (Fig. 12)	1	37.16	56.34	-	1.49	5.01	-	-	-	-	-	NiO+CoO
	2	49.47	13.99	10.88	14.62	5.9	1.17	1.73	2.25	-	-	$(Ni,Co)Al_2O_4+NiCr_2O_4+CrTaO_4+NiTiO_3+W_{20}O_{58}$
	3	49.11	14.92	11.6	13.83	5.83	0.41	2.52	1.78	-	-	$(Ni,Co)Al_2O_4+NiCr_2O_4+CrTaO_4+W_{20}O_{58}$
	4	47.14	2.26	43.26	0.94	0.98	-	-	-	5.41	-	α-$Al_2O_3+HfO_2$
	5	-	66.74	3.69	11.42	13.23	0.66	2.68	0.35	-	1.23	Poor Al-zone
1100°C/500 h (Fig. 13)	1	31.15	62.69	-	1.52	4.64	-	-	-	-	-	NiO+CoO
	2	37.23	24.83	10.63	13.07	6.65	1.82	2.02	3.74	-	-	$(Ni,Co)Al_2O_4+NiCr_2O_4+CrTaO_4+NiTiO_3+W_{20}O_{58}$
	3	47.12	17	20.58	8.47	4.89	0.14	-	1.8	-	-	$(Ni,Co)Al_2O_4+NiCr_2O_4+CrTaO_4$
	4	44.79	4.46	44.3	0.83	1.49	-	-	-	4.12	-	α-$Al_2O_3+HfO_2$
	5	-	66.06	3.5	11.23	13.27	0.67	2.81	1.18	-	1.28	Poor Al-zone

At 1000°C, a mixed-oxide scale formed on the surface of superalloy after 200 h and 500 h oxidation. The bright oxide particles were observed in some regions beneath the outer layer NiO with a small amount of CoO. The bright oxide particles observed beneath the outer layer indicated the Ta-rich phase that is $CrTaO_4$. (Ni,Co)O has higher growth rate compared to other oxides where it can be recognized from the XRD pattern as seen in Fig. 4. This high growth rate will result in overgrowth of NiO. Furthermore, the solid phase reaction among the simple oxides were occurred during isothermal oxidation process, leading to the formation of $(Ni,Co)O + Al_2O_3 \rightarrow (Ni,Co)Al_2O_4$ [19], $Cr_2O_3 + NiO$

→ $NiCr_2O_4$ [17], NiO + TiO_2 → $NiTiO_3$ [17] and Cr_2O_3 + Ta_2O_5 → $CrTaO_4$ [18]. However, some isolated particles of HfO2 did form in this study. It is believed that these zones develop via the outward diffusion of hafnium. HfO_2 is slightly more stable than alumina and the HfO_2 precipitates are visible adorning within the inner α-Al_2O_3 as mentioned in Table 1 and 2. The HfO_2 precipitate [20] was derived from the reaction of HfC + O_2 → HfO_2 + CO_2. The oxygen oxidizes aluminum and the HfO_2 precipitates mantled with α-Al_2O_3 layer. As the alumina scale grows inward it incorporates the hafnium precipitates whereby the α-Al_2O_3 is permeated with HfO_2. Meanwhile, the gray background appeared at the center of oxide scale revealed that the area is mainly consisted of spinels (Ni,Co)Al_2O_4 and $NiCr_2O_4$ with a small amount of $CrTaO_4$ after 200 h but $CrTaO_4$ was not observed after 500 h oxidation as presented in Table 1. This is possibly due to the decrease of the oxygen activity at the scale/superalloy interface after the mixed-oxide scale formed, which then facilitates the selective oxidation of Al, leading to the formation of further α-Al_2O_3. The inner α-Al_2O_3 crystals grew laterally and finally converged to form a dense inner scale. The inner layer becomes thick and mainly composed of α-Al_2O_3 and secondarily HfO_2.

Basically, the oxidation at 1100°C was similar to that at 1000°C but the transient-oxidation period was more shortened than that at 1000°C because of the rapid build-up of the inner α-Al_2O_3 resulting from fast outward diffusion of Al in the superalloy compared to the oxidation at 1000°C. The spinel (Ni,Co)Al_2O_4 and α-Al_2O_3 was predominant oxide formed in the intermediate layer and the inner scale, respectively. A minor content of (Ni,Co)O is still found after oxidation for 200 h and 500 h at 1100°C as shown in Fig. 5. This is due to the rapid consumption of (Ni,Co)O derived from the formation of (Ni,Co)Al_2O_4 by the acceleration of solid-state diffusion reaction between the transient NiO and α-Al_2O_3 at high temperature circumstances. The prolongation of oxidation time results in the increasing the thickness of the oxide scales which motivates the change in chemical composition of its oxides [21]. The NiO grew become larger forming a blocky morphology as seen in Fig. 9b. Thereunto, the outward diffusion of Ni is impeded by the swift outgrowth of the inner α-Al_2O_3 layer, and NiO growth is eventually hindered.

4. CONCLUSIONS

The isothermal oxidation behavior of a second generation Ni-base single crystal superalloy at 1000°C and 1100°C was investigated. The following conclusions can be withdrawn from this investigation:

(i) The oxidation kinetics characteristic of a second generation Ni-base single crystal superalloy at 1000°C and 1100°C obeys the parabolic law. It is primarily controlled by the growth of the inner α-Al_2O_3 layer.

(ii) The Ni-base single crystal superalloy showed better oxidation resistance at 1000°C than that at 1100°C because the K_p value at 1000°C is lower compared to that at 1100°C.

(iii) Mostly, the oxide scale formed on the surface of Ni-base single crystal superalloy after 200 h and 500 h oxidation can be divided into three regions, an outer layer, an intermediate layer, and a continuous inner layer.

ACKNOWLEDGEMENT
The authors are grateful to Prof. Koichi Kitazono -in the Department of Aerospace Engineering, Faculty of System Design, Tokyo Metropolitan University, Hino Campus, Japan- to support us for the XRD examination.

References

1. D. W. MacLachlan, D. M. Knowles, *Mater. Sci. Eng. A.*, 302 (2001) 275.
2. J. S. Bae, J. H. Lee, S. S. Kim, C. Y. Jo, *Script. Mater.*, 45 (2001) 503.
3. K. Shirvani, M. Saremi, A. Nishikata, T. Tsuru, *Corros. Sci.*, 45(5) (2003) 1011.
4. B. Pieraggi, F. Dabosi, *Mater. Corros.*, 38 (1987) 584.
5. M. H. Li, X. F. Sun, T. Jin, H. R. Guan, Z. Q. Hu, *Oxid. Met.*, 60 (2003) 195-210.
6. W. Gao, Z.W. Li, Z. Wu, S. Li, Y.D. He, *Intermetallics*, 10 (2002) 263–270.
7. M. D. Ferdinando, A. Fossati, A. Lavacchi, U. Bardi, F. Borgioli, C. Borri, C. Giolli, A. Scrivani, *Surf. Coat. Technol.*, 204 (2010) 2499–2503.
8. G. E. Fuchs, *Mater. Sci. Eng. A.*, 300 (2001) 52.
9. H. Zhou, Y. Ro, H. Harada, Y. Aoki, M. Arai, *Mater. Sci. Eng. A.*, 381 (2004) 20.
10. N. Czech, F. Schmitz, W. Stamm, *Surf. Coat. Technol.*, 68/69 (1994) 17.
11. L. R. Liu, T. Jin, N. R. Zhao, Z. H. Wang, X. F. Sun, H. R. Guan, Z.Q. Hu, *Mater. Sci. Eng. A.*, 385 (2004) 105.
12. X. M. Hou, K. C. Chou, *J. Eur. Ceram. Soc.*, 29 (2009) 517.
13. B. Wang, C. Sun, J. Gong, R. Huang, L. Wen, *Corros. Sci.*, 46 (2004) 519.
14. T. F. An, H. R. Guan, X. F. Sun and Z.Q. Hu, *Oxid. Met.*, 54 (2000) 301.
15. J. Huang, H. Fang, X. Fu, F. Huang, H. Wan, Q. Zhang, S. Deng, and J. Zu, *Oxid. Met.*, 53 (2000) 273.
16. S. Giggins, F. S. Pettit, *J. Electrochem. Soc.*, 118 (1971) 1782.
17. K. Hauffe, G.H. Meier, Oxidation of Metals, Plenum, New York, 1966.
18. O. Kubaschewski, B.E. Hopkins, Oxidation of Metals and Alloys, Butterworths, London, 1962.
19. B. Pieraggi, *Mater. Sci. Eng.*, 88 (1987) 199.
20. Per Kofstad, High Temperature Corrosion, Elsevier Applied Science, London and New York, 1988.
21. F. H. Latief, K. Kakehi, X. Fu, *Int. J. Electrochem. Sci.*, 7 (2012) 7608.